Climatological Aspects of Notable Tornado Events in Chile

JULIO C. MARÍN,[a,b] FELIPE GUTIÉRREZ,[a] VITTORIO A. GENSINI,[c] BRADFORD S. BARRETT,[d] DIANA POZO,[a,b] MARTÍN JACQUES-COPER,[e,f,g] AND DANIEL VELOSO-AGUILA[h]

[a] *Department of Meteorology, Universidad de Valparaíso, Valparaíso, Chile*
[b] *Centro de Estudios Atmosféricos y Cambio Climático, Universidad de Valparaíso, Valparaíso, Chile*
[c] *Department of Earth, Atmosphere, and Environment, Northern Illinois University, DeKalb, Illinois*
[d] *Raleigh, North Carolina*
[e] *Department of Geophysics, Universidad de Concepción, Concepción, Chile*
[f] *Center for Climate and Resilience Research, Universidad de Concepción, Concepción, Chile*
[g] *Center for Oceanographic Research COPAS Coastal, Universidad de Concepción, Concepción, Chile*
[h] *Department of Atmospheric Science, Colorado State University, Fort Collins, Colorado*

(Manuscript received 7 October 2023, in final form 28 April 2024, accepted 9 May 2024)

ABSTRACT: Tornadoes in Chile seem to develop in what are called "high-shear, low-CAPE" (HSLC) environments. An analysis of convective parameters from the ERA5 reanalysis during 16 notable tornadoes in Chile showed that several increased markedly before the time of the reports. The significant tornado parameter (STP) was able to discriminate the timing and location of the tornadoes, even though it was not created with that goal. We established thresholds for the severe hazards in environments with reduced buoyancy (SHERBE) parameter (≥ 1) and the STP (≤ -0.3) to further identify days favorable for tornado activity in Chile. The SHERBE and STP parameters were then used to conduct a climatological analysis from 1959 to 2021 of the seasonal, interannual, and latitudinal variations of the environments that might favor tornadoes. Both parameters were found to have a strong annual cycle. The largest magnitudes of STP were found to be generally confined to south-central Chile, in agreement with the (sparse) tornado record. The probability of a day with both SHERBE and STP values beyond their thresholds was greatest between May and August, which aligns with the months with the most tornado reports. The number of days with both SHERBE and STP beyond their respective thresholds was found to fluctuate interannually. This result warrants further study given the known interannual variability of synoptic and mesoscale weather in Chile. The results of this study extend our understanding of tornado environments in Chile and provide insight into their spatiotemporal variability.

KEYWORDS: South America; Severe storms; Tornadoes

1. Introduction

Severe convective storms (those containing large hail, destructive convective wind gusts, and/or tornadoes) are intrinsic components of Earth's energy balance, often bearing devastating consequences on human life, infrastructure, and ecosystems. While these phenomena are more frequently found and studied in regions such as central Europe and the Great Plains of the United States, their occurrence has been documented across varied geographies in the midlatitudes of both the Northern and Southern Hemispheres (Brooks et al. 2003; Tippett et al. 2015; Brooks et al. 2019). In particular, the South American continent—with its complex topography and unique geography—experiences a relatively high frequency of extreme convection, especially east of the extratropical Andes (Durkee and Mote 2010; Romatschke and Houze 2010; Matsudo and Salio 2011; Rasmussen et al. 2014; Bruick et al. 2019; Moraes et al. 2020; Kumjian et al. 2020; Piersante et al. 2021; Schumacher et al. 2021), where tornadoes are among the severe convective storm threats (Schwarzkopf 1988; Nunes et al. 2011; Silva Dias 2011; Rasmussen et al. 2014; Dos Santos et al. 2023; Veloso-Aguila et al. 2024; Lopes and Nascimento 2024). In contrast, west of the extratropical Andes (i.e., Chile), a unique blend of coastal and mountainous terrain, juxtaposes with influences from the South Pacific marine layer to the west and the Andes to the east to occasionally create favorable environments for cold-season tornadoes.

Although tornadoes in Chile may not attain the frequency and intensity observed in regions like the central U.S. Great Plains or southeast South America, several notable cases have been documented. For example, the 30 and 31 May 2019 tornadoes in Los Angeles and Talcahuano and Concepción in south-central Chile were particularly well recorded and found to be associated with an anomalous 500-hPa thermal trough and a related surface cyclone to the west of Chile (Barrett et al. 2020; Vicencio et al. 2020; Marín et al. 2021). Those events seem to have occurred as part of a larger outbreak as other tornadoes were also reported in that part of the country (Vicencio et al. 2020). The atmosphere on both days was characterized by weak buoyancy on the order of 200–500 J kg^{-1} mixed-layer (lowest 100 hPa) convective available potential energy (MLCAPE) and significant deep-layer and low-level shear. The latter may have been largely influenced by a strong low-level jet potentially enhanced by flow blocking by the Andes (Barrett et al. 2020). This was later confirmed by several high-resolution sensitivity experiments that changed the height of the topography, obtaining as a result a large decrease in the bulk shear and the storm-relative helicity in the simulations with reduced topography (Marín et al. 2021). In addition, the sea surface temperature

Corresponding author: Julio C. Marín, julio.marin@meteo.uv.cl

DOI: 10.1175/MWR-D-23-0249.1

(SST) of the southeastern Pacific seems to also modulate storm severity in Chile via an influence on atmospheric instability (Marín et al. 2021).

The synoptic and mesoscale regimes commonly referred to as "high-shear, low-CAPE" (HSLC) environments seem to be common in areas of the world geographically similar to Chile, including California, southern Australia, and the British Isles (Monteverdi and Quadros 1994; Hanstrum et al. 2002; Clark 2009; Sherburn and Parker 2014; Mulder and Schultz 2015). Anticipating tornadoes in these environments is notoriously difficult (Sherburn et al. 2016) since they tend to be small in horizontal dimensions compared to those in "classic" environments and due to the shallow nature of the near-surface vertical vorticity associated with vertical pressure perturbations that are often not well resolved by numerical models (Wade and Parker 2021). In addition, HSLC environments favor a quasi-linear convective system (QLCS) storm mode (Thompson et al. 2012), which presents a distinct challenge to the operational warning process (Davis and Parker 2014; Ellis et al. 2020). The mesocyclonic circulations that occur with such a convective mode are often transitory and vertically shallow. This results in greater difficulty from a Doppler radar remote sensing perspective as these circulations often form and decay during only a few volume scans.

The topic of severe storms and tornadoes in Chile is relatively new. The few existing studies on Chilean tornadoes provide some insight into the synoptic and mesoscale conditions of these storms and the factors that may have influenced storm severity. However, many aspects of tornado activity remain unclear and need to be better understood. In this study, we first investigate climatological aspects of selected events from a database of tornado and waterspout reports in Chile. This includes attempts to better understand their frequency, variability, and characteristic atmospheric environments. The tornado and waterspout databases, along with the reanalysis dataset used for sampling historical environmental vertical profiles, are described in the next section. Results are then presented, including an analysis of the seasonal, interannual, and latitudinal variability of tornadoes in Chile. Two key parameters are analyzed in the hours immediately preceding and following each event. The results conclude with a presentation of trends in these parameters since 1959. Discussion and an overall summary of the results are provided thereafter.

2. Data and methods

a. Tornado reports in Chile

As previously mentioned, the number of tornado reports in Chile is small compared to other parts of the world. The low number of reports may be in part related to the fact that these events may happen over sparsely populated regions of the country. During the most recent decades, the increasing availability of mobile devices (e.g., smartphones) is likely a factor in an increase in the number of these reports. A database of tornado and waterspout reports has been recently created by several researchers, forecasters, students, and weather enthusiasts, using newspapers, official reports, multimedia, and social media evidence. A large number of them can be found in Bastías Curivil (2019) and in a wiki page (Wikipedia 2019). It includes reports as old as 1633, but most of them are after the twentieth century. This is an unofficial database, unlike in the United States where tornadoes are studied and rated on the F/EF scale by personnel in the National Weather Service.

Tornadoes and waterspouts in Chile tend to concentrate over the latitudinal band 30°–45°S and during the austral fall and winter months (Figs. 1a,b). Tornadoes were most frequently reported in the fall and the beginning of winter (Fig. 1c) over a relatively small latitudinal band (36°–42°S), whereas waterspouts are more likely in winter months. From the relatively small number of tornado events in the Chilean database, we selected 16 cases. These reports were all from after 1980 and had a known time of occurrence. We analyzed them in greater detail in the first part of this study using modern reanalysis. The date, intensity rating, location, and coordinates of the 16 selected tornado cases are provided in Table 1.

b. Reanalysis dataset

The fifth major global reanalysis (Hersbach et al. 2020) produced by the European Centre for Medium-Range Weather Forecasts (ECMWF) (ERA5) was used to assess the modeled best-guess convective environment for all 16 cases in Table 1. The ERA5 data were also used to create a 63-yr climatology of tornado-relevant variables. ERA5 has been shown to compare favorably to radiosonde observations in the United States and Europe (Taszarek et al. 2021b) and has been used in several recent tornado environment studies in the United States (Coffer et al. 2019; Gensini et al. 2021; Taszarek et al. 2021a; Pilguj et al. 2022), Europe (Rodríguez and Bech 2021; Taszarek et al. 2021a; Shikhov et al. 2022; Istrate et al. 2023; Pilorz et al. 2024), and South America (Dos Santos et al. 2023; Veloso-Aguila et al. 2024), including in Chile (Vicencio et al. 2020).

In general, ERA5 has shown good agreement with observations for studies focused on Chile (Schauwecker et al. 2022; González-Reyes et al. 2023; Lagos-Zúñiga et al. 2024). However, we are aware that ERA5 might have difficulties in resolving mesoscale processes, particularly due to the fact that the study area covers complex terrain features, including atmosphere–ocean contrasts along the coast (Demortier et al. 2021) and boundary layer processes in the Chilean Central Valley (Muñoz et al. 2022). ERA5 data were obtained at 3-hourly intervals for 24 pressure levels from 100 to 1000 hPa on an approximately 0.25° horizontal latitude–longitude grid (bilinearly interpolated from the native Gaussian grid) and analyzed for an area between 20°–56°S and 85°–68°W for the period 1959–2021.

c. Convective parameters

Several convective parameters often used to diagnose tornado potential were calculated from the ERA5 reanalysis data using the R package thundeR (Taszarek et al. 2021b), which can be downloaded from https://bczernecki.github.io/thundeR/. The thundeR package calculates 201 convective parameters from vertical profiles of pressure, geopotential height, air and dewpoint temperatures, and u and v wind components. Table 2 describes the convective parameters examined in this study,

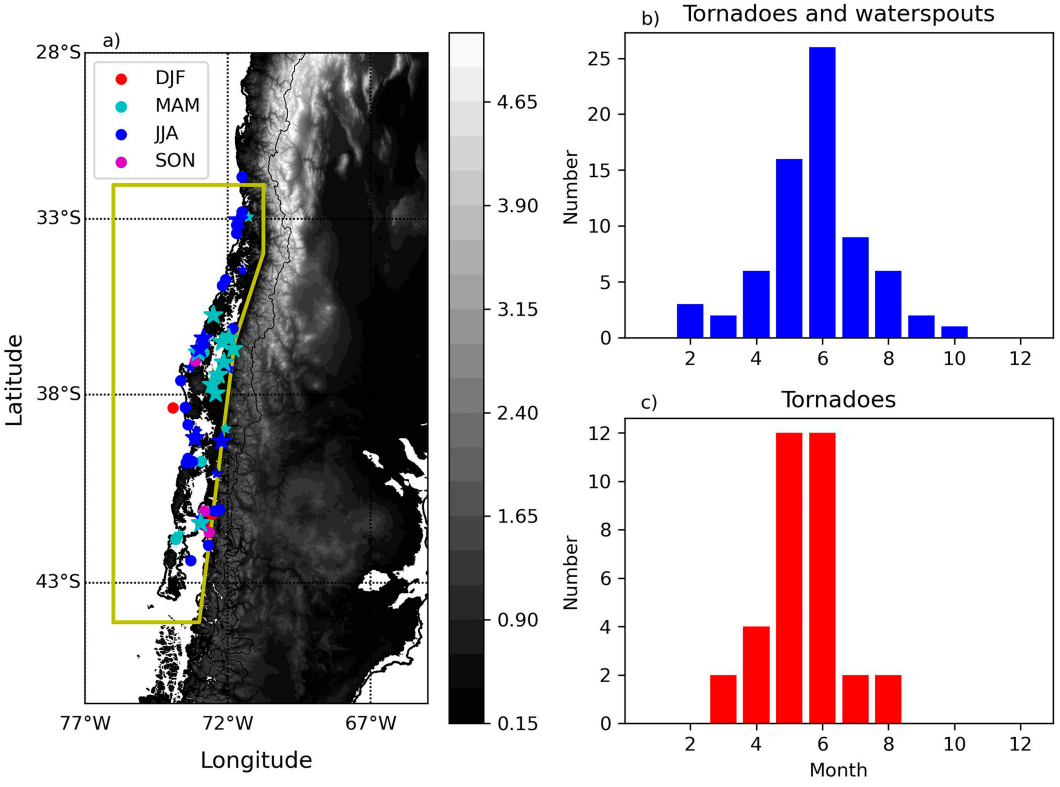

FIG. 1. (a) Location of tornado (stars) and waterspout (circles) reports in Chile between 1633 and 2021, identified by season. Terrain elevation (km) is shaded in grayscale. The 16 tornado cases described in Table 1 are drawn in a larger size. The yellow polygon encloses the masked area used in the analysis removing the Andes topography. (b) Seasonal distribution of tornado and waterspout reports in Chile. (c) As in (b), but only showing tornado reports.

which were calculated at each time interval and grid point of the study domain. Since ERA5 provides the mixing ratio as an initial state field, the dewpoint temperature was calculated using the expression given in Romps (2021).

Tornadoes in Chile seem to develop in HSLC convective environments associated with extratropical cyclones moving eastward from the Pacific Ocean. Sherburn and Parker (2014) found that combining the 0–3-km and 700–500-hPa lapse rates

TABLE 1. Dates and locations of 16 tornadoes reported in Chile analyzed in this study. The intensity ratings on the (enhanced) Fujita scale are also reported if known.

Date	(E)F scale	Latitude (°S)	Longitude (°W)	Location
18 May 1981	F3	36.425	71.958	San Carlos, Ñuble
19 Jun 1991	—	33.036	71.630	Valparaíso
14 Jun 2010	—	36.72	72.976	Penco, Lirquén
14 Jun 2010	—	36.422	72.857	Vegas de Itata
7 Jun 2011	EF3	39.267	72.217	Villarica
31 May 2013	EF3	36.425	71.958	San Carlos, Ñuble
22 Mar 2018	—	41.443	72.945	Puerto Montt
30 May 2019	—	36.533	72.2	Quilelto, San Carlos
30 May 2019	—	37.104	72.134	San Miguel de Itata
30 May 2019	—	36.726	71.81	Coihueco, Ñuble
30 May 2019	EF2	37.45	72.33	Los Angeles
30 May 2019	—	37.958	72.432	San Andrés
31 May 2019	EF1	36.82	73.05	Gran Concepción
31 May 2019	—	35.775	72.505	Chanco, Maule
25 Apr 2020	—	37.718	72.576	Renaico
9 Jun 2021	—	39.178	73.164	Toltén

TABLE 2. Convective parameters examined in this study.

Abbreviation	Name	Units
MLCAPE	100-hPa mixed-layer CAPE	J kg^{-1}
EBSMU	Bulk wind shear from the most unstable parcel level upward to 40%–60% of the equilibrium level height	m s^{-1}
MLCIN	100-hPa mixed-layer convective inhibition	J kg^{-1}
MLLCL	Height of the lifting condensation level, derived from the 100-hPa mixed-layer parcel	m
LR03	0–3-km lapse rate	K km^{-1}
LR75	700–500-hPa lapse rate	K km^{-1}
SRH500	Storm-relative helicity calculated using the Bunkers left-moving storm motion for the 0–500 m	m^2 s^{-2}
SHERBE	Sherburn and Parker (2014); using effective shear	Dimensionless
STP	Significant tornado parameter; Thompson et al. (2003), Coffer et al. (2019)	Dimensionless

with a shear magnitude in a composite parameter is the most skillful at discriminating between HSLC significant severe convection and nonsevere convection in the United States. The parameters were called severe hazards in environments with reduced buoyancy (SHERB), and a number of them were developed depending on whether a fixed or variable layer was used in the wind shear calculation. In this study, we tested the SHERBS3 and SHERBE parameters, which use the 0–3-km shear magnitude and the effective shear magnitude, respectively, to analyze how well they identify conditions favorable for tornadoes in Chile. Since similar results for both SHERBE and SHERBS3 were found, we only present the results from SHERBE defined as

$$\text{SHERBE} = (\text{EBSMU}/27\,\text{m s}^{-1}) \times (\text{LR03}/5.2\,\text{K km}^{-1}) \times (\text{LR75}/5.6\,\text{K km}^{-1}), \quad (1)$$

where the EBSMU is the effective bulk shear of the most unstable layer, calculated upward to 40%–60% of the equilibrium level height. The LR03 and LR75 represent the 0–3-km and 700–500-hPa lapse rates, respectively.

The significant tornado parameter (STP) is another widely used composite parameter (Thompson et al. 2003) to discriminate significant and nontornadic environments for right-moving supercells and has been used in various climatological applications (Grams et al. 2012; Gensini and Brooks 2018; Gensini and Bravo de Guenni 2019). The thundeR package version used, by default, calculates the STP in the Northern Hemisphere (storm-relative helicity calculated with a Bunkers right-moving storm motion). Therefore, STP was calculated based on Coffer et al. (2019), but the 0–500-m storm-relative helicity term was calculated using the Bunkers left-moving storm motion to characterize Southern Hemisphere conditions:

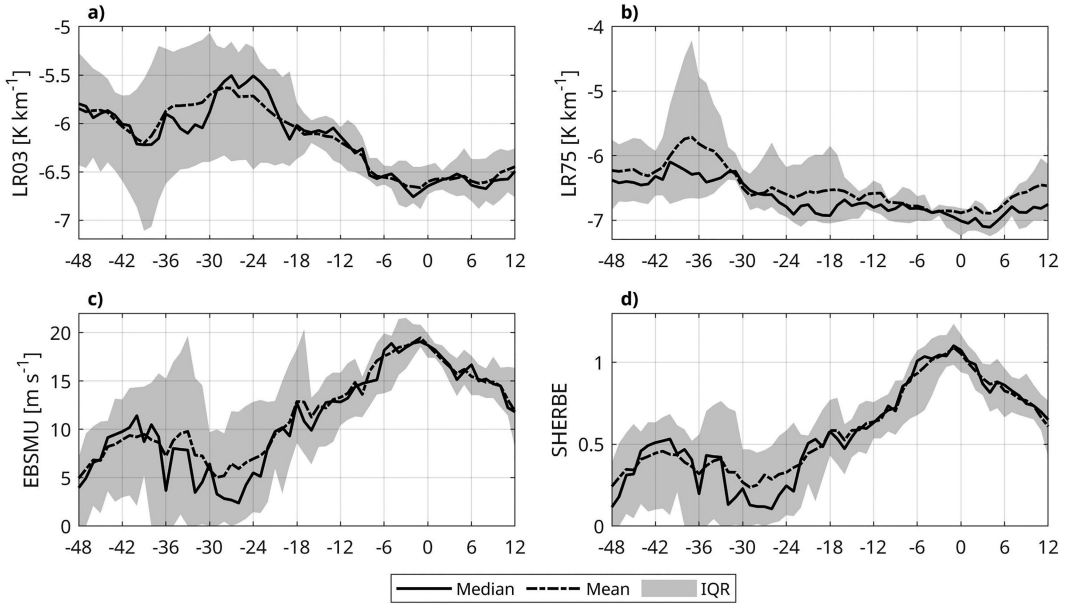

FIG. 2. Time evolution of (a) LR03, (b) LR75, (c) EBSMU, and (d) SHERBE parameters from $T - 48$ to $T + 12$ h relative to the tornado report. Black solid and dashed lines represent the median and mean, respectively, of maximum values in a 0.5° × 0.5° domain, averaged over 16 tornado cases. The colored area represents the interquartile range (IQR).

$$\text{STP} = (\text{MLCAPE}/1500\,\text{J kg}^{-1}) \times [(2000 - \text{MLLCL})/(1000\,\text{m})] \times (\text{SRH500}/75\,\text{m}^2\,\text{s}^{-2}) \times (\text{EBSMU}/20\,\text{m s}^{-1}) \times [(200 + \text{MLCIN})/(150\,\text{J kg}^{-1})], \quad (2)$$

where MLCAPE represents the mixed-layer (lowest 100 hPa) CAPE, MLLCL is the lifting condensation level of the mixed layer, SRH500 is the storm-relative helicity over the 0–500-m layer, and MLCIN represents the convective inhibition of the mixed layer. The STP calculation also includes the following conditions: 1) The MLLCL term is set to 1 when values are <1000 m and 0 when values are >2000 m; 2) the MLCIN term is set to 1 when values are >-50 J kg^{-1} and set to 0 when values are <-200 J kg^{-1}; and 3) the EBSMU term is capped at 1.5 for values >30 m s^{-1} and set to 0 when values are <12.5 m s^{-1}.

In this study, we defined each day as starting at 0000 UTC and ending at 2100 UTC, thus using eight ERA5 intervals for each diurnal cycle. We did not find any notable difference in the results by defining a day from, for example, 1200–0900 UTC.

3. Results

a. *Evolution of convective parameters during tornado events*

For each of the 16 tornado cases (Table 1), the temporal evolution of the aforementioned convective variables was examined from 48 h before ($T - 48$ h) to 12 h after ($T + 12$ h) the time of the tornado report. We calculated the maximum values in a 0.5° × 0.5° domain centered at the ERA5 grid point closest to the tornado report. Averaging over all cases was performed to capture the mean convective environment near these events.

For most cases, there is a steady steepening of LR03 beginning ≈30 h prior to tornado report time (Fig. 2a). LR03 remains between −6 and −7 K km^{-1} for more than 12 h after the tornado report. The temporal evolution of the LR75 shows values in excess of −6 K km^{-1} over the majority of the period (Fig. 2b). Therefore, both the LR03 and LR75 show conditions increasingly favorable for low- and midtropospheric buoyancy leading up to the time of each tornado report. In all cases, the effective bulk shear of the most unstable air parcel (EBSMU) greatly increases from $T - 30$ h to a mean value near 20 m s^{-1} at $T - 0$ h (Fig. 2c). This increase is quite abrupt for some of the analyzed cases. Maximum EBSMU values even larger than 20 m s^{-1} are found in several cases near the time of the report. The temporal evolution of SHERBE is very similar to that of EBSMU for all 16 tornado cases, increasing from values close to 0 two days before the event to values >1 at $T - 0$ h. This increase confirms that the bulk wind shear modulates the SHERBE parameter in our HSLC environments. In the following sections, we will use a SHERBE threshold of ≥1 to identify days with mesoscale environments favorable for tornadoes.

MLCAPE also showed an increase roughly beginning $T - 12$ h (Fig. 3a) to maximum values even larger than 400 J kg^{-1} in some cases. The 0–500-m storm-relative helicity (SRH500) also increases in magnitude starting around $T - 48$ h to mean values around −200 m^2 s^{-2} at $T - 15$ h (Fig. 3b). Among the five variables used in calculating the STP parameter, MLCAPE, EBSMU, and SRH500 are the ones that most notably influence it. As a result, the STP parameter reaches its maximum value at almost the same time as MLCAPE and EBSMU. In contrast, the SRH500 reaches its peak several hours earlier for reasons not yet fully understood. This might be partly associated with the SRH500 being affected by the nocturnal low-level jet, but this requires further, in-depth, analysis.

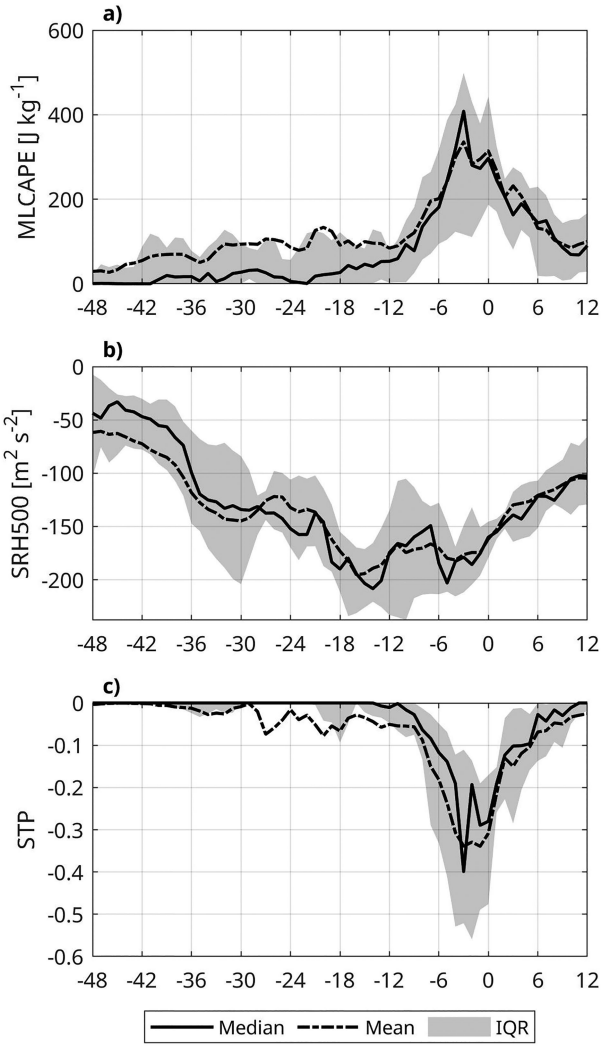

FIG. 3. Time evolution of (a) MLCAPE, (b) SRH500, and (c) STP from $T - 48$ to $T + 12$ h relative to each of the reported tornado start times. Black solid and dashed lines represent the median and mean, respectively, of maximum values in a 0.5° × 0.5° domain, averaged over 16 tornado cases. The colored area represents the IQR.

Despite being created with the aim of identifying environments most favorable for significant tornadoes in the United States, STP does an admirable job capturing the occurrence of the 16 selected tornado events, slowly increasing from $T - 48$ to $T - 24$ h. STP has a sharp increase between $T - 9$ and $T - 0$ h (Fig. 3c). The STP threshold found to statistically discriminate between significant and nontornadic supercells in the United

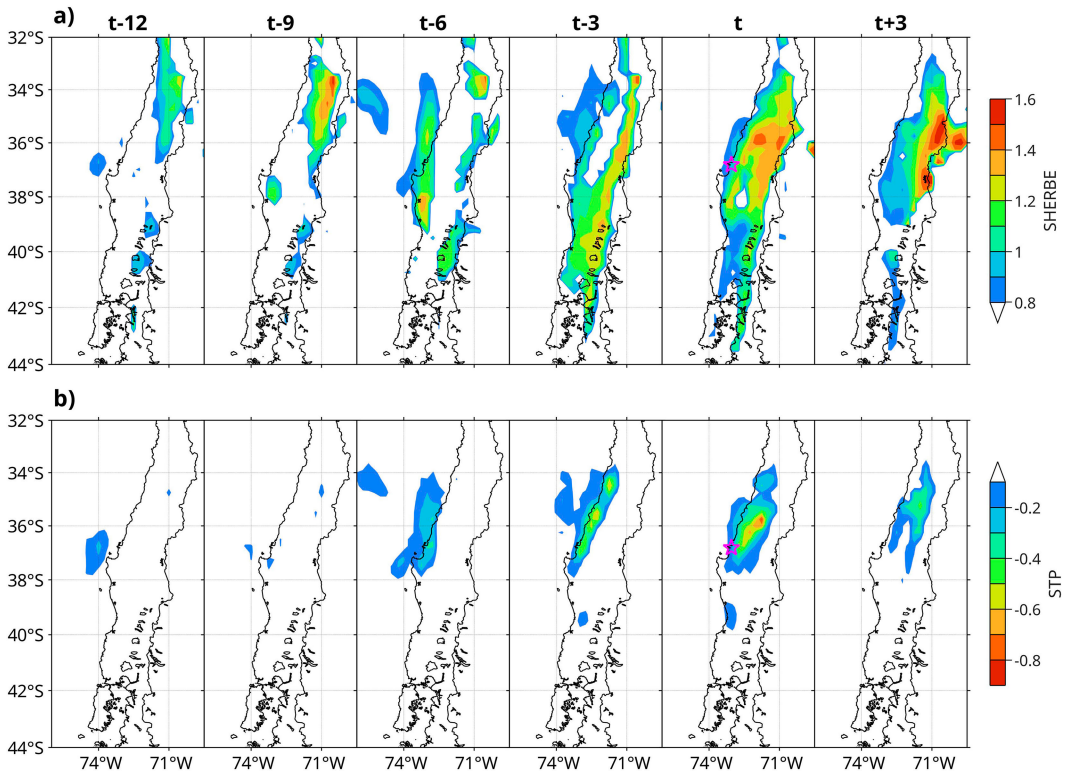

FIG. 4. Spatial evolution of (a) SHERBE and (b) STP for the 1800 UTC 31 May 2019 tornado case near Concepción (pink star on $T - 0$ h column panels).

States was 1 (Thompson et al. 2003, 2004). Maximum values for the 16 tornado events analyzed here vary between −0.1 and −0.9 at grid points near each tornado. In the following sections, we will use an STP threshold of −0.3 (in conjunction with the aforementioned SHERBE value ≥ 1) to identify mesoscale environments favorable for tornadoes in Chile.

We calculated how extreme the 1.0 and −0.3 thresholds for SHERBE and STP, respectively, were over continental Chile (terrain within the yellow polygon of Fig. 1a) between 1959 and 2021 to support the use of these values. The analysis showed that the −0.3 STP threshold is beyond the 99th percentile over continental Chile if we take positive and negative values into account, and it is above the 98th percentile if we only take negative values into account. Moreover, the SHERBE threshold (1.0) is also above the 99th percentile if we take all values into account, and it is above the 97th percentile if we only take positive values into account. This result indicates that these are extreme values. We also examined the time series of the same variables presented in Figs. 2 and 3, but for the nearest grid point to the reports over the same domain. Although the time evolution is noisier, they are similar (not shown).

On 30 and 31 May 2019, a localized tornado outbreak (seven reported tornadoes) occurred in south-central Chile. The spatial distribution of SHERBE and STP parameters was plotted for this case from $T - 12$ to $T + 3$ h relative to the time an EF-1 tornado hit Concepción at 1800 UTC 31 May 2019 (Fig. 4). A relatively large area of SHERBE values > 1 (with a maximum > 1.3) was located in continental Chile between 32° and 37°S starting at $T - 12$ h (Fig. 4a). Other smaller areas with values >0.9 appear over the Pacific Ocean (near 36.8°S, 74°W), close to the reported tornado location (pink star on Fig. 4) and over the Andes in southern Chile. These areas of relatively large SHERBE values continue to increase in size by $T - 9$ h, showing more intense SHERBE values. From $T - 6$ to $T - 0$ h, SHERBE values > 0.8 cover almost all of continental Chile between 33° and 44°S, with maximum values approaching 1.5. These magnitudes increase at $T + 3$ h, although with a decreased spatial extent.

Twelve hours before the tornado report, a relatively small area of STP values < −0.2 was located over the Pacific Ocean adjacent to Concepción (Fig. 4b). Negative STP values spread parallel to the coast and become more negative until the event, with values at or below −0.6. At the time of the tornado, a large area of negative STP covers Concepción and part of continental Chile between 34° and 38°S, concentrated between the coast and the western foothills of the Andes. These conditions continue 3 h after the tornado, but similar to SHERBE, the region of negative STP is smaller in spatial extent.

We analyzed the evolution of SHERBE and STP parameters for the other 15 tornado days in Chile, and they featured, in general, similar results (not shown). The SHERBE parameter was positive from several hours before to the time of the tornadoes, covering not only the locations where the tornadoes were reported but also a larger area including the Andes. On the

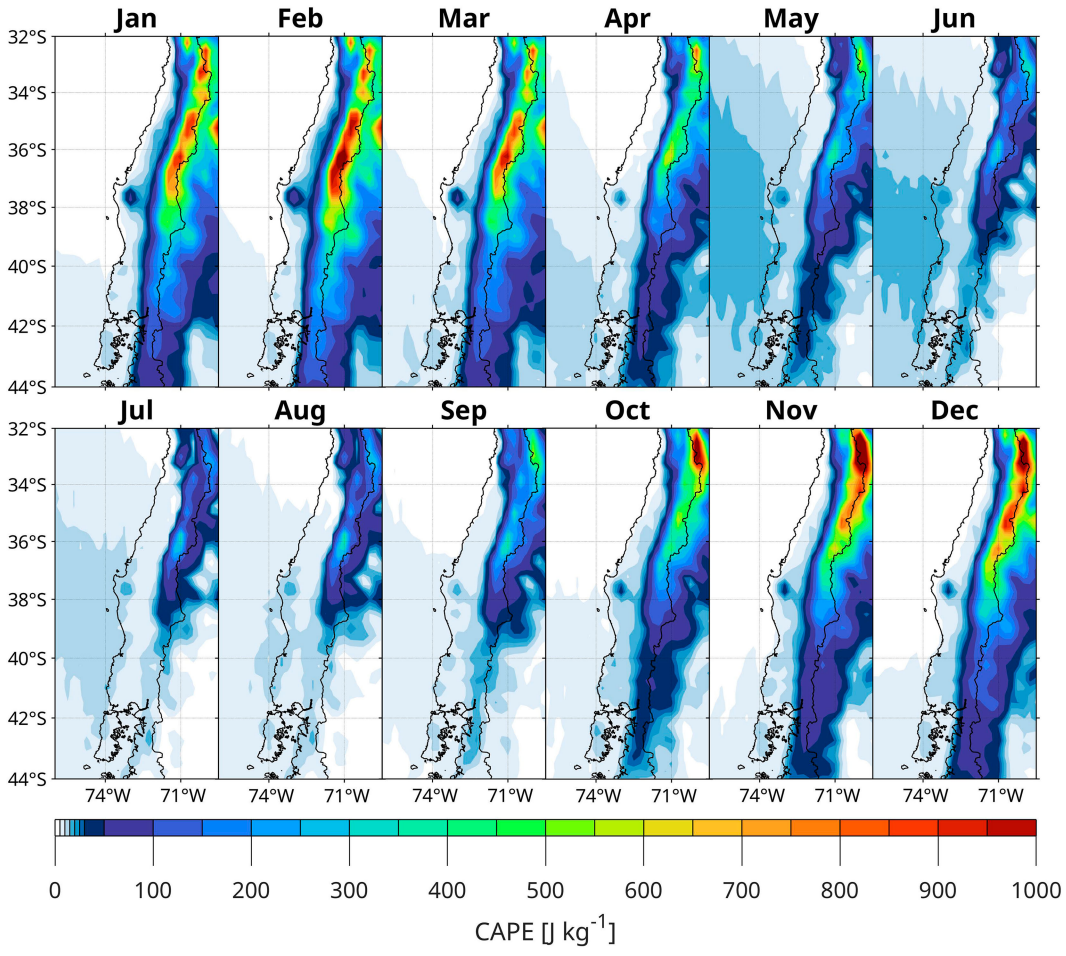

FIG. 5. Monthly distribution of mean MLCAPE (1959–2021).

contrary, the region of negative STP tended to be more localized, covering the location of each tornado and adjacent parts of continental Chile away from the western foothills of the Andes.

b. *Seasonality of convective parameters*

Results in the previous subsection showed a large increase in the effective shear, MLCAPE, and SRH500 near the times when 16 tornadoes were reported in Chile. An evaluation of the monthly evolution of these variables, which as far as we are aware has not been done so far, will help to better understand the seasonality of tornado occurrence in Chile.

The spatial distribution of monthly mean MLCAPE (Fig. 5), averaged over the period 1959–2021, shows large values (mainly during austral summer) over the Andes and the eastern (Argentinean) foothills, at their leeward side. However, our focus is on the region covering the Pacific Ocean and continental Chile to the west of the Andes. There, the greatest MLCAPE values are located in a northwest-to-southeast band over the Pacific Ocean and continental Chile. This band of relatively higher MLCAPE shifts equatorward and reaches its northernmost position and maximum values over the ocean in May and June. This may be associated with cooler air masses over relatively warmer and moister conditions at and near the surface in those months compared with subsequent winter months, thus favoring the development of deeper convection during the passage of extratropical cyclones over the region (Barrett et al. 2009; Pozo et al. 2023).

The spatial distribution of the monthly mean storm-relative helicity for a left-moving storm, calculated between the surface and 500 m (SRH500), shows a small region of negative values over the Chilean coast between 34° and 38°S and in continental Chile south of 42°S during most of the austral summer and spring months (Fig. 6). This area of negative SRH500 values slowly shifts to the north along the coast and along continental Chile during austral fall and winter (Fig. 6). The SRH500 reaches its northernmost extension (around 35°S) between May and August, and in those months, it also reaches its largest magnitudes over continental Chile. As is indicated in Fig. 5, this coincides with the months with the largest mean unstable conditions over south-central Chile. Thus, the collocation of maximum values of these variables in south-central Chile in these months favors the development of deeper convection and storm severity. The maxima also coincide with the annual peak in tornado reports in that part of Chile (Fig. 1).

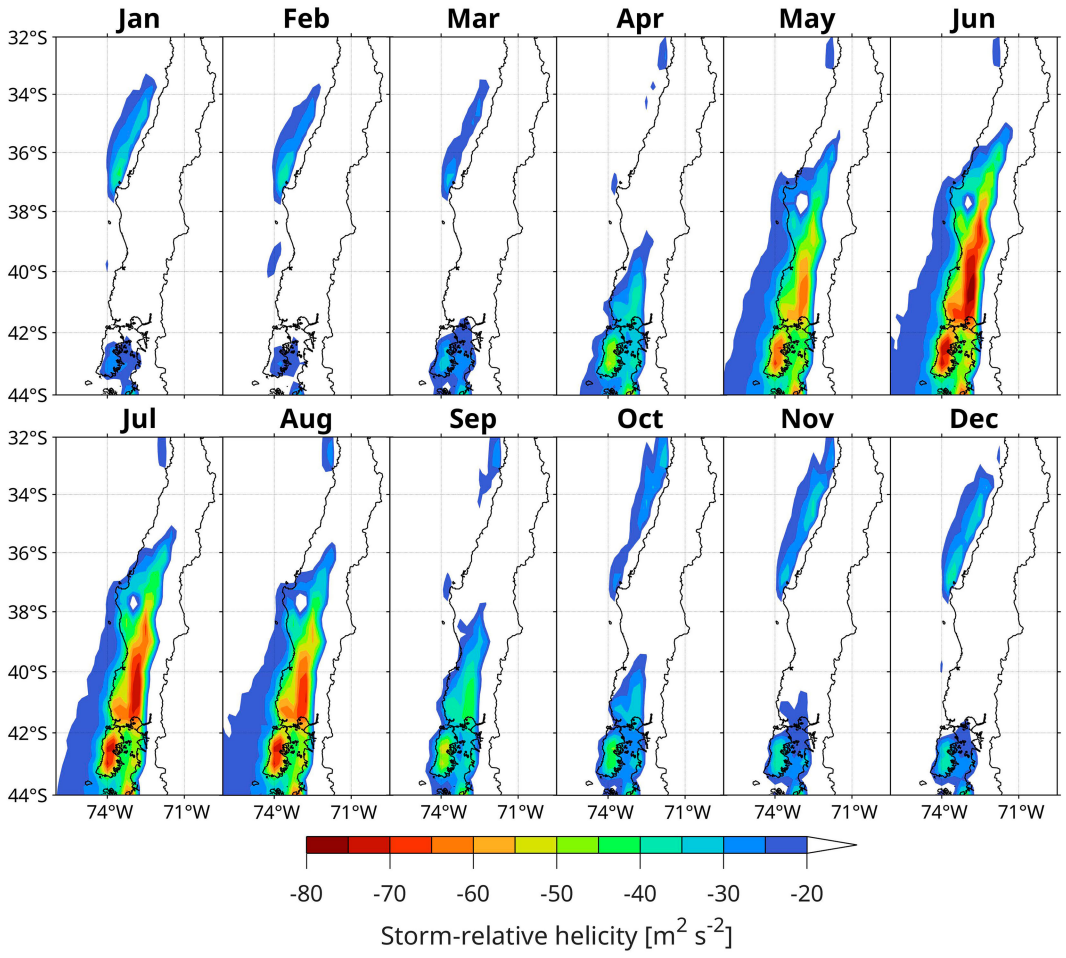

FIG. 6. As in Fig. 5, but for 0–500-m storm-relative helicity (storm motion calculated using Bunkers left mover).

Since we mentioned that SHERBE values ≥ 1 and STP values ≤ -0.3 are extremes in their respective distributions, we also analyze the monthly evolution of conditions exceeding the SHERBE and STP thresholds. SHERBE values ≥ 1 are present during the whole year over the Andes and to the east in Argentina (Fig. 7). Sherburn and Parker (2014) noted that values above 1 can be found in locations where severe convection will not occur, for example, in environments characterized by large convective inhibition or in mountainous terrain. This may be the case over the Andes. Areas with SHERBE values ≥ 1 over continental Chile start to appear on average in May, and they persist until September between 34° and 44°S. This translates to an average of 3–4 days per month between May and September with environments favorable for tornadoes over continental Chile.

The monthly mean horizontal distribution of the number of days with STP ≤ -0.3 shows smaller, localized areas in continental Chile reaching this threshold in the 3-month periods of January–March and October–December (Fig. 8). The number of days surpassing the -0.3 threshold increases in the austral fall and winter months, as do their spatial extents. Days with STP values below -0.3 are located between 34° and 44°S in continental Chile, to the west of the Andes. May shows the largest number of days surpassing the STP threshold, followed by July. Two spatial "hotspot" regions show the largest number of times with STP values ≤ -0.3 from May to August: 1) an area located between the Cordillera de la Costa (coastal range) and the Andes (near 38°S, 72°W), and 2) the Chiloé Island (42.7°S, 74°W), both of which are present nearly 1 day per month. The first hotspot area coincides with the region where more tornadoes occur in Chile, whereas waterspouts have been reported in the Chiloé Island (see Fig. 1a). Overall, STP seems to delineate tornado environments even better than SHERBE by more clearly highlighting their spatial locations over continental Chile and reducing the number of days the SHERBE threshold is met over the Andes. The next analysis is focused on times when the STP and SHERBE surpass the -0.3 and 1.0 thresholds, respectively, over the Chilean territory within the yellow polygon in Fig. 1a.

Based on these climatologies, the monthly probability of having a day with 10, 20, or 50 grid points within the study domain (32°–44°S, 75°–72°W) with SHERBE values ≥ 1 during the 1959–2021 period was calculated (Fig. 9a). However, for this and the following analysis on the SHERBE and STP parameters

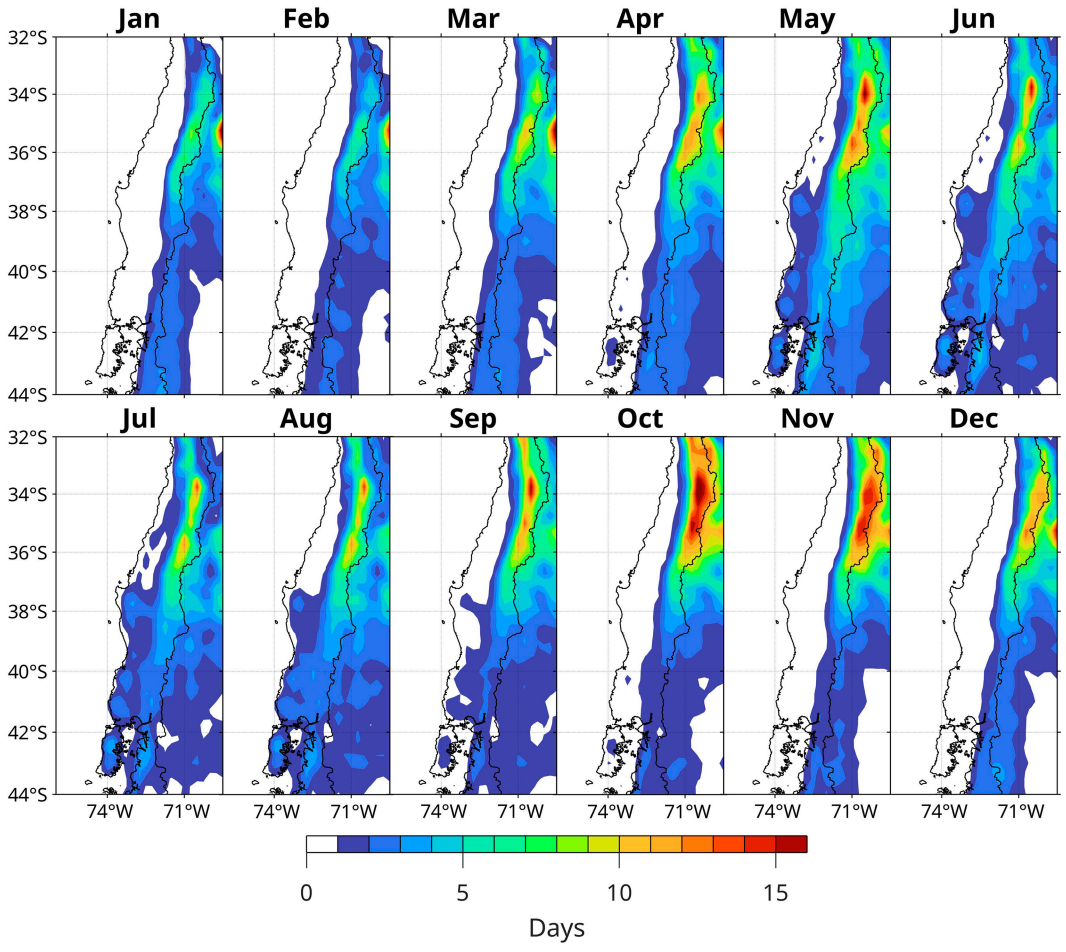

FIG. 7. Average number of days per month with SHERBE values ≥ 1 for the period 1959–2021. A day is defined as starting at 0000 UTC and ending at 2100 UTC.

in this section, we only included grid points over continental Chile, to the west of the Andes, excluding the Andes and western Argentina. Thus, the 10, 20, and 50 grid points represent ~1%, ~2%, and ~6%, respectively, of the entire domain. The probabilities of having 10 or 20 grid points in continental Chile with SHERBE values above 1 show a similar annual variation, with values above 33% and 23% per day, respectively, between May and October, decreasing the rest of the year. The probability of 50 grid points exceeding the SHERBE threshold shows a slightly different annual evolution, with values increasing from less than 5% in January to a maximum larger than 15% per day in June, decreasing afterward.

Similar to the analysis of SHERBE, the probabilities for days with STP ≤ −0.3 were also calculated by month (Fig. 9b). The greatest probabilities of days with STP ≤ −0.3 are found from May to August, with May showing more than 5%, 3%, and 1% of days with at least 10, 20, or 50 grid points below −0.3, respectively. These lower probabilities (as compared to SHERBE) reflect the more restricted spatial coverage of areas with favorable STP for tornadoes in Chile. For smaller spatial areas (10 or 20 grid points) having an STP value ≤ −0.3, the probability increases from January to a maximum in May and then decreases the remainder of the year. However, the probability of larger areas (≥50 grid points) having STP values ≤ −0.3 has a bimodal distribution, with the most significant maximum occurring in May and a second maximum in July.

The latitudinal variation of the probability of having a day with 10, 20, or 50 grid points with SHERBE values ≥ 1.0 during the 1959–2021 period was also examined by dividing the study domain into latitude belts 32°–36°S, 36°–40°S, and 40°–44°S. The largest probabilities for smaller areas (10 and 20 grid points) having SHERBE values ≥ 1.0 occur in the latitude band 32°–36°S instead of between 36° and 44°S (Figs. 10a–c). The probabilities of favorable SHERBE days are also larger between April and November in that latitudinal band. The probability of having a day with 10, 20, or 50 grid points with SHERBE values ≥ 1.0 is highest between May and August over the latitudinal band 36°–44°S, which agrees with Chile's seasonal variation of reported tornadoes. It is important to remember, however, that while tornado reports in Chile seem to concentrate in the latitudinal band 36°–40°S (Fig. 1a), the probability of having a day with 10 and 20 grid points with SHERBE values ≥ 1.0 is the smallest in that latitudinal band.

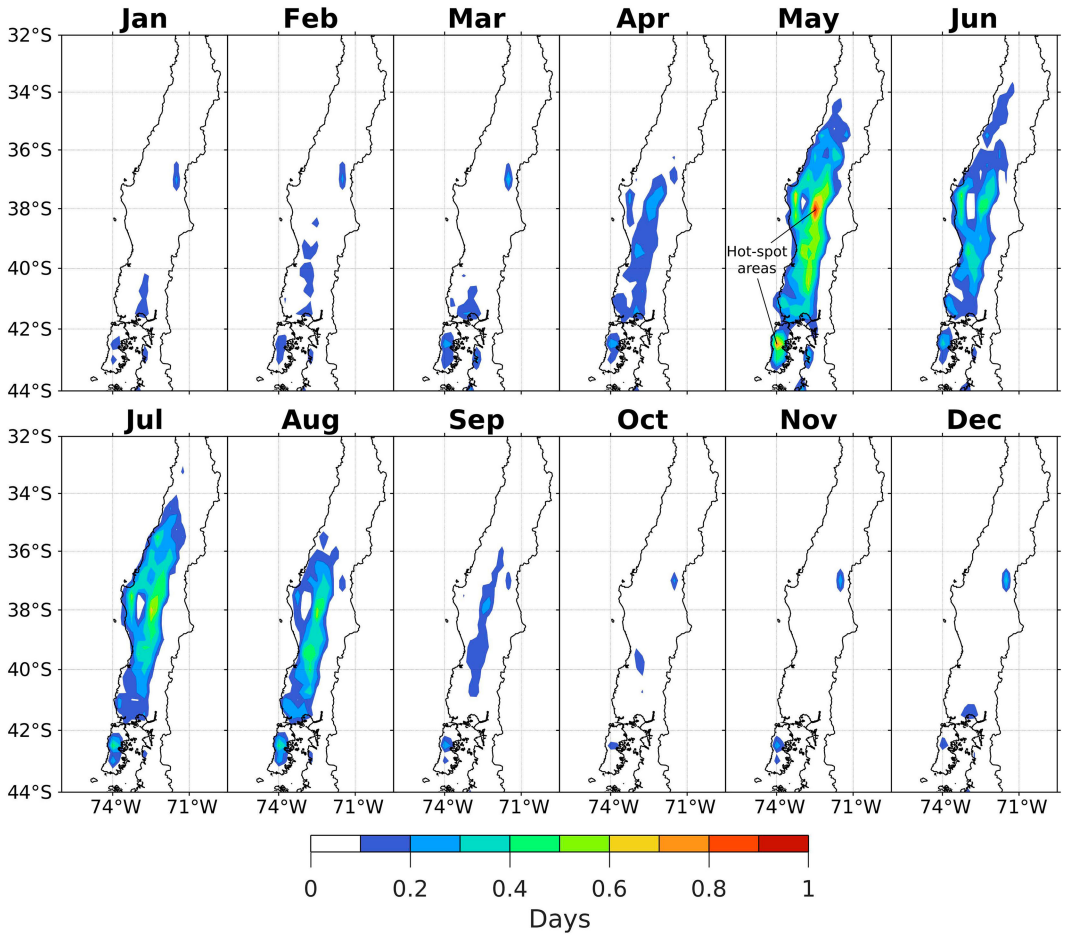

FIG. 8. Average number of days per month with STP values ≤ −0.3 for the period 1959–2021. A day is defined as starting at 0000 UTC and ending at 2100 UTC.

For STP, the largest probabilities were found between 36° and 40°S and the lowest between 32° and 36°S (Figs. 10d–f). The seasonality of this probability changes depending on the latitudinal band analyzed. It is at maximum in July for latitudes 32°–36°S, whereas it is at maximum in May for latitudes south of 40°S. This result even holds for the probability of 10, 20, and 50 grid points reaching STP ≤ −0.3. The seasonality of the probability of favorable STP days between 36° and 40°S is close to that shown for the whole domain, but an apparent bimodal seasonality is seen for areas ≥20 grid points, with greatest probabilities in May and July.

To gain more insight into the higher-frequency variability, the 5-day probability of having 10, 20, or 50 grid points with SHERBE values ≥ 1 was calculated (Fig. 11a). In general, probabilities increase to values around 30%, 20%, and 10% between May and October for 10, 20, and 50 grid points, respectively, exceeding SHERBE values ≥ 1. This result may indicate bimodality in the seasonality of probabilities for smaller areas (10 grid points), with maximum values in the 2-month periods May–June and September–October. Most of the tornado reports occur in May and June, but the probability of large coverage of high SHERBE values is similar in both 2-month periods.

The five-daily probability of days that exceed the STP threshold is the greatest between May and August. In general, the seasonality of STP also follows a bimodal distribution, with the highest probabilities in May and July and lower ones at the end of June and the beginning of July. The bimodal distribution is clearer for larger spatial areas (50 grid points), but not so for small areas (≤20 grid points). The number of tornado reports in Chile largely coincides with the period with the highest probability of environments that favor tornadoes. In addition, waterspouts have been reported in Chile between May and June, but their seasonal reports seem not to correspond to the five-daily STP probability as well as the number of tornadoes. This result should be studied further.

c. *Interannual variability and trends*

The number of days per year having 10, 20, or 50 grid points with SHERBE values ≥ 1 within the study domain varies significantly between 1959 and 2021 (Fig. 12a), not showing a clear indication of a trend for the three analyzed areas based on this parameter. To confirm the latter, we calculated the trend in the number of days with HSLC environments based on the number of days per year having SHERBE values ≥ 1 at each grid point

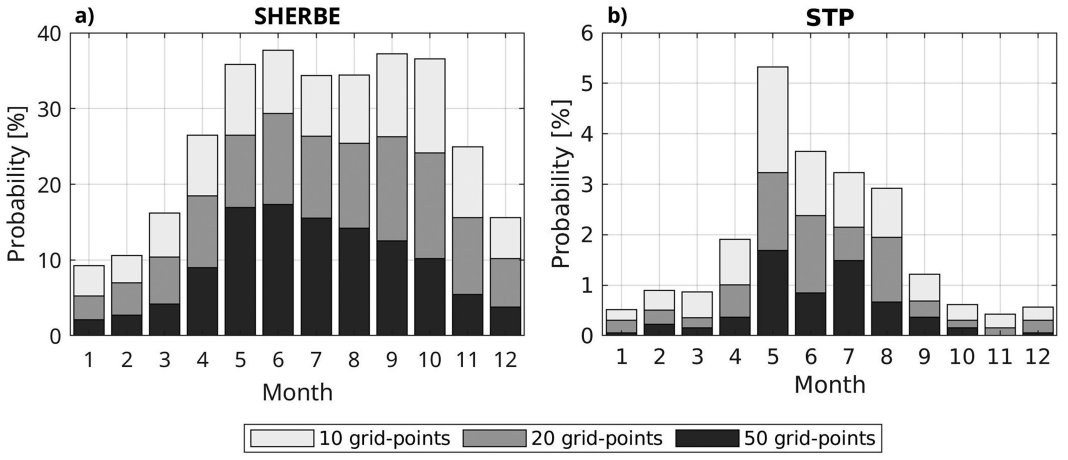

FIG. 9. Monthly evolution of the probability of having a day with 10, 20, or 50 grid points with (a) a SHERBE value ≥ 1 and (b) an STP value ≤ −0.3 over the domain 32°–44°S, 75°–72°W for the period 1959–2021.

over the study domain for the period 1959–2021 using a Mann–Kendall test (Fig. 13a). A statistically significant negative trend is found in a narrow band over the Andes between 35° and 38°S, whereas a statistically significant positive trend in HSLC environments is shown over most of Chile south of 44°S. We also analyzed whether the overall trend in the number of days with SHERBE values ≥ 1 changes if it is calculated separately for the first (1959–89) and the second half (1990–2021) of the study period. During the first half of the period (Fig. 13b), there is a statistically significant small negative trend over several grid points of the Pacific Ocean. On the other hand, two broad areas of statistically significant positive trends from 1959 to 1989 are shown over continental Chile between 35° and 41°S and south of 44°S, respectively (Fig. 13b). The second half of the study period (Fig. 13c) only shows isolated grid points with statistically significant negative trends over continental Chile.

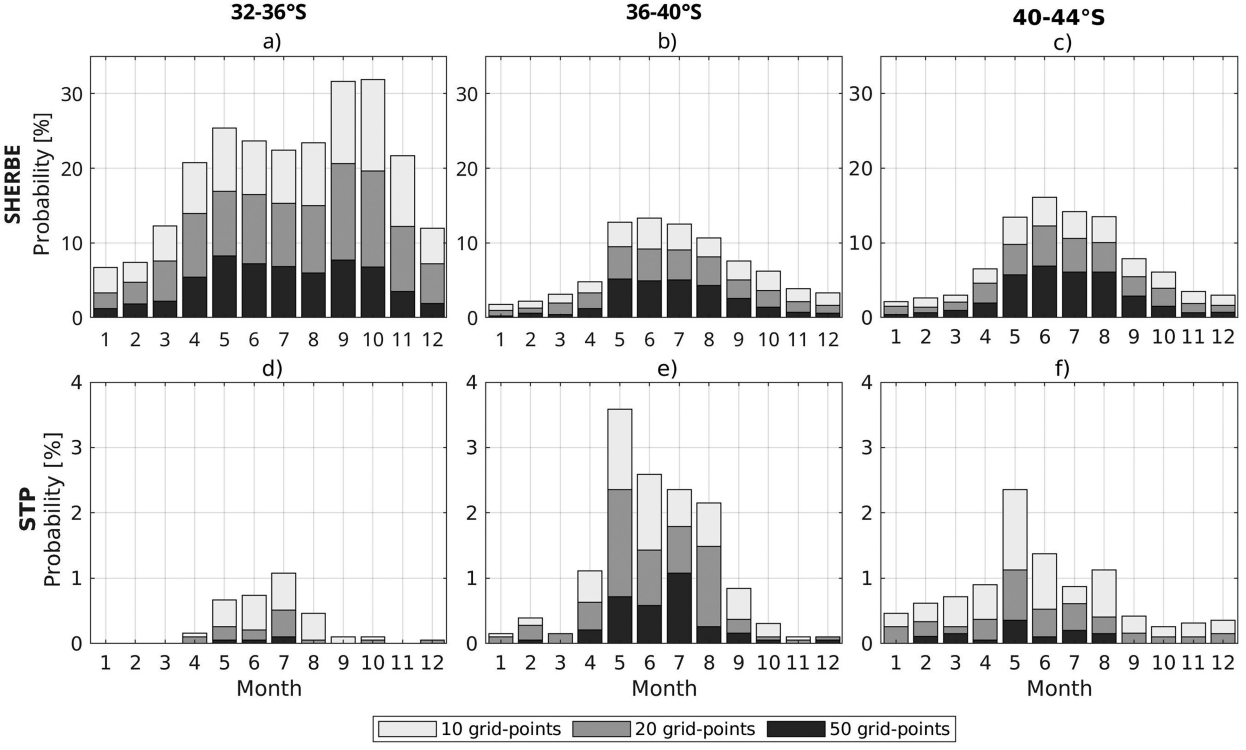

FIG. 10. Monthly evolution of the probability of having a day with 10, 20, or 50 grid points with SHERBE values ≥ 1 over latitude belts (a) 32°–36°S, (b) 36°–40°S, and (c) 40°–44°S during the period 1959–2021. (d)–(f) As in (a)–(c), respectively, but for STP values ≤ −0.3.

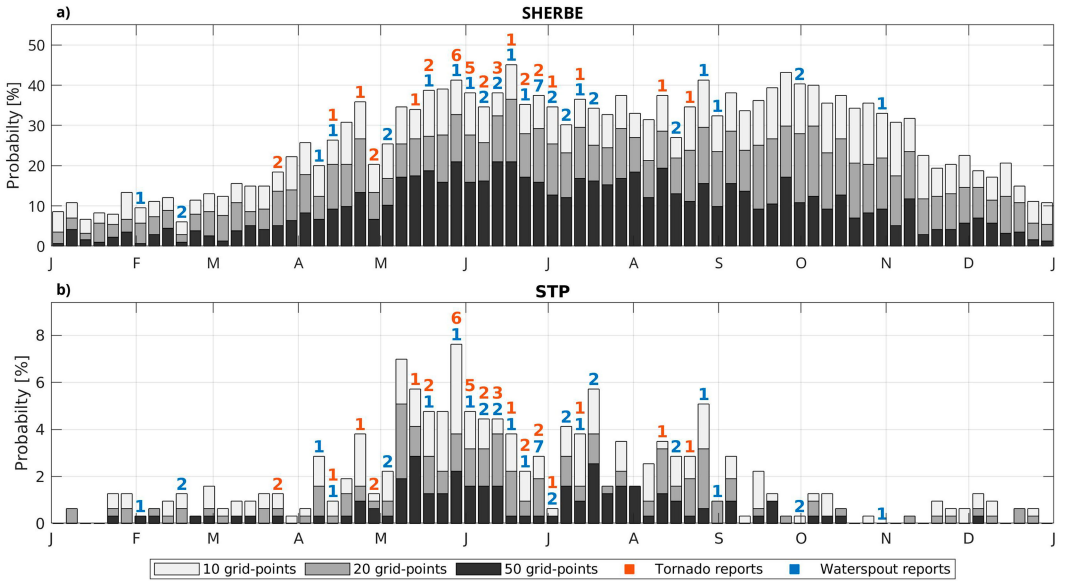

FIG. 11. Annual cycle of five-daily probability values of having a day with 10, 20, or 50 grid points over the study domain with (a) SHERBE values ≥ 1 and (b) STP values ≤ −0.3, averaged over the period 1959–2021. The red and blue colors above the bars represent the number of tornadoes and waterspouts, respectively, that have been reported in Chile within every 5-day period.

The number of days per year having 10, 20, or 50 grid points with STP values ≤ −0.3 also shows large interannual variability (Fig. 12b). In this case, a clearer signal seems more evident using STP as a measure of environments favorable for tornadoes, mainly for the larger areas (≥20 grid points). The number of days with STP exceeding the threshold seems to have increased from 1959 toward the end of the 1980s, with a subsequent decrease until 2021. As has been shown, the Pacific decadal oscillation (PDO) changed from its cold toward its warm phase in the mid-1970s (Hare and Mantua 2000; Meehl et al. 2009; Newman et al. 2016), and the related Pacific basin-wide climate shift had several impacts on the South American mean conditions (Jacques-Coper and Garreaud 2015). Particularly, the subsequent abrupt intensity decrease in the southeast

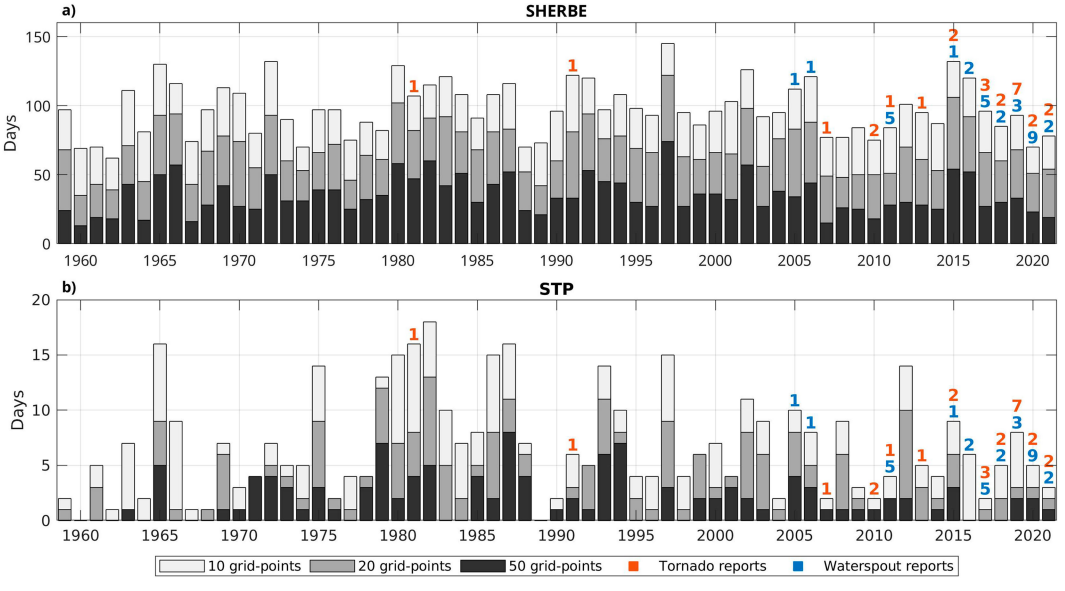

FIG. 12. Annual number of days having 10, 20, or 50 grid points with (a) a SHERBE value ≥ 1 and (b) an STP value ≤ −0.3 over the study domain during the period 1959–2021. The red and blue colors above the bars represent the annual number of tornadoes and waterspouts, respectively, that have been reported in Chile.

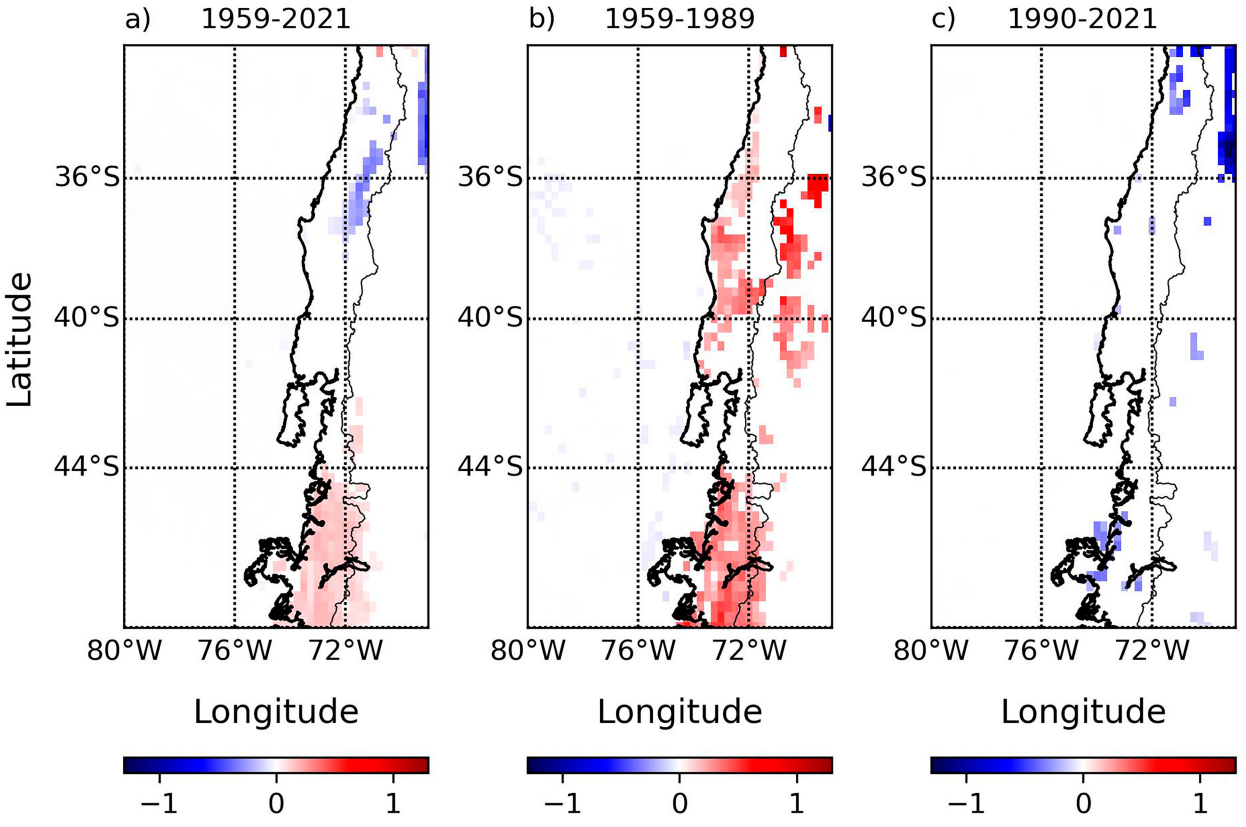

FIG. 13. Horizontal distribution of calculated trends (number of days per year) in the frequency of SHERBE values ≥ 1 during (a) 1959–2021, (b) 1959–89, and (c) 1990–2021 periods. Periods with no statistically significant trend values (p values > 0.05) are masked in white.

Pacific subtropical anticyclone (SPSA) favored a higher frequency of wet years over central Chile (Quintana and Aceituno 2012), a fact particularly evident in the 1980s. However, the intensity of the SPSA gradually recovered toward the 2000s (Falvey and Garreaud 2009; Jacques-Coper and Garreaud 2015), eventually reducing synoptic-scale cyclone activity over the study area. These aspects might be associated with each of the multidecadal trends observed in the convective parameters in this work (Figs. 13 and 14). However, the PDO's possible role in modulating the conditions that favor tornadoes in Chile is a topic for future work.

The number of tornadoes and waterspouts reported in Chile per year was also included in Fig. 12 to find out whether there is a consistency in the number of days reaching the aforementioned thresholds and the number of reported tornadoes. The figure shows that despite some years having a large number of reported cases showing a relatively large number of days above the thresholds, most of the reported cases occur in the last 10 years of the study period. This highlights the fact that population growth over previous sparsely populated areas, along with greater access to recording tools and social media, may impact the Chilean tornado database. Some tornadoes in the past likely went undetected.

The SHERBE > 1 trend analysis was repeated for STP ≤ −0.3 (Fig. 14a). Only isolated grid points over the Pacific Ocean show a very small positive trend over 63 years. However, different results are obtained when we calculate this trend for the first half (1959–89) of the study period. A statistically significant positive trend is noted over a large band in continental Chile between 36° and 42°S, with trend values larger than 0.1 days per year over that period. A smaller region of larger values (about 0.2 days per year) is indicated in the hotspot region between 36° and 40°S. The trend analysis calculated for the second half of the overall period (1990–2021) only shows a few grid points with statistically significant negative trends, somewhat similar to that shown for the whole study period.

It is important to mention that we repeated the analysis for the seasonal, intraseasonal, and interannual evolution of times and areas where STP and SHERBE values independently surpass their thresholds. We focused on the times and areas where STP values ≤ −0.3 were collocated with SHERBE values ≥ 1. We aimed to find out whether the combination of the two parameters could better determine the areas for possible tornado occurrence and thus potentially improve upon the skill of either the STP or SHERBE parameters in isolation. We did not find any notable differences between the results from collocated parameters and those when we used the STP parameter alone. It seems the combination of SHERBE and STP parameters restricts the locations favorable for tornadoes in Chile, similar to STP alone but with a noisier signal.

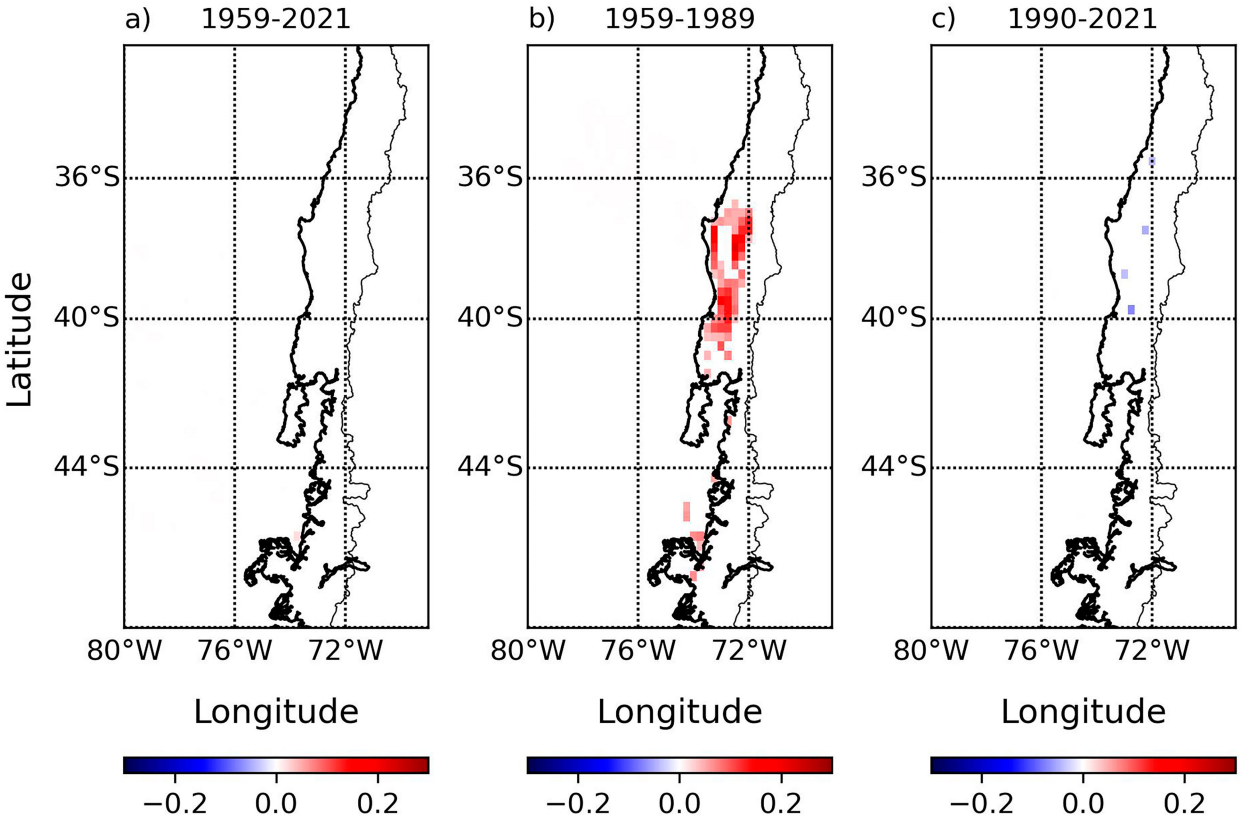

FIG. 14. As in Fig. 13, but for STP values ≤ −0.3.

4. Discussion and conclusions

In this study, we used the ERA5 reanalysis to examine variables known to influence tornado potential for 16 cases of notable tornadoes in Chile. For most cases, low- and midlevel lapse rates showed a steady steepening leading up to the time of each tornado, indicating increasingly favorable low- and midtropospheric buoyancy. The effective bulk shear, CAPE, and storm-relative helicity variables also showed a relatively large increase in magnitude from hours before to the time of tornadoes. In addition to these variables, the composite parameters SHERBE and STP were examined for the life cycle of each event, given their known ability to discriminate tornado environments in other regions of the world.

The SHERBE parameter seems to nicely show maximum values around the times of each tornado. However, relatively large SHERBE values not only cover locations where tornadoes were reported but also cover portions of the Andes itself. On the other hand, the STP parameter seems to discriminate the tornado environments better than SHERBE by capturing the timing of their occurrences and more clearly delimiting their spatial locations over continental Chile. This is so despite STP not being created with the aim of analyzing HSLC- or QLCS-type environments but those for the most significant supercell tornadoes in the U.S. Great Plains.

From these 16 events, thresholds of SHERBE (≥1) and STP (≤−0.3) were used along with CAPE and low-level storm-relative helicity to create climatologies of favorable tornado environments from 1959 to 2021. The analysis of the temporal evolution of convective parameters revealed a strong seasonality in Chile's tornado-prone regions. MLCAPE, SRH500, and STP showed increased values between late austral fall and winter months (May–August), which coincided with the peak tornado season in Chile. The climatological analysis also revealed that the region between 36° and 40°S latitude appeared to be a hotspot for tornado frequency, with the highest number of tornado reports. This and the seasonality of tornado reports in Chile were much better represented by the STP parameter than the SHERBE parameter.

Interannual variability in the STP and SHERBE was strongly evident, with fluctuations in the number of days per year with environments favorable for tornadoes. While there was not a clear trend in the number of days with SHERBE values ≥ 1 for the whole domain of study, STP values ≤ −0.3 showed an increase from 1959 to the late 1980s, followed by a decrease thereafter. However, the number of days per year having SHERBE values ≥ 1 and STP values ≤ −0.3 shows statistically significant increases in continental Chile during the period 1959–80 over the latitudinal band 36°–40°S. Possible modulations of tornado-favorable conditions by large-scale circulations such as ENSO, MJO, or the PDO, which have been previously reported to affect environmental conditions in south-central Chile, are a subject of future research.

Overall, this study highlights the convective conditions leading to tornado events in Chile and provides valuable insights into their probability, seasonality, interannual variability, and spatiotemporal trends. These findings advance our knowledge of tornado-prone regions outside of other well-studied regions and can be valuable for improving tornado awareness, prediction, and preparedness in Chile and similar climatological regions.

Acknowledgments. Marín, Pozo, and Gutiérrez acknowledge support from the Centro de Estudios Atmosféricos y Cambio Climático (CEACC), Universidad de Valparaíso. Marín and Pozo acknowledge support from ANID/Fondecyt Project 1211898. Gensini acknowledges support from the U.S. National Science Foundation Award 2048770. Jacques-Coper acknowledges support from ANID/FONDAP/1522A0001 and ANID/FB210021.

Data availability statement. ERA5 reanalysis data were obtained from the European Centre for Medium-Range Weather Forecasts (ECMWF), Copernicus Climate Change Service (C3S), using the Climate Data Store Application Program Interface (CDS API; https://cds.climate.copernicus.eu). The tornado database was created using the information in Bastías Curivil (2019) and in the wiki page: https://es.wikipedia.org/wiki/Anexo:Tornados_en_Chile. The convective parameters analyzed in the manuscript were calculated using the R package thundeR (Taszarek et al. 2021b), which can be downloaded at https://bczernecki.github.io/thundeR/.

REFERENCES

Barrett, B. S., R. Garreaud, and M. Falvey, 2009: Effect of the Andes Cordillera on precipitation from a midlatitude cold front. *Mon. Wea. Rev.*, **137**, 3092–3109, https://doi.org/10.1175/2009MWR2881.1.

——, J. C. Marin, and M. Jacques-Coper, 2020: A multiscale analysis of the tornadoes of 30–31 May 2019 in south-central Chile. *Atmos. Res.*, **236**, 104811, https://doi.org/10.1016/j.atmosres.2019.104811.

Bastías Curivil, C. A., 2019: Influencia de los procesos geológicos en la cosmovisión mapuche, entre concepción y chiloé. Tesis Pregrado, Universidad de Chile, https://repositorio.uchile.cl/handle/2250/175020.

Brooks, H. E., J. W. Lee, and J. P. Craven, 2003: The spatial distribution of severe thunderstorm and tornado environments from global reanalysis data. *Atmos. Res.*, **67–68**, 73–94, https://doi.org/10.1016/S0169-8095(03)00045-0.

——, and Coauthors, 2019: A century of progress in severe convective storm research and forecasting. *A Century of Progress in Atmospheric and Related Sciences: Celebrating the American Meteorological Society Centennial*, *Meteor. Monogr.*, No. 59, Amer. Meteor. Soc., https://doi.org/10.1175/AMSMONOGRAPHS-D-18-0026.1.

Bruick, Z. S., K. L. Rasmussen, and D. J. Cecil, 2019: Subtropical South American hailstorm characteristics and environments. *Mon. Wea. Rev.*, **147**, 4289–4304, https://doi.org/10.1175/MWR-D-19-0011.1.

Clark, M. R., 2009: The southern England tornadoes of 30 December 2006: Case study of a tornadic storm in a low CAPE, high shear environment. *Atmos. Res.*, **93**, 50–65, https://doi.org/10.1016/j.atmosres.2008.10.008.

Coffer, B. E., M. D. Parker, R. L. Thompson, B. T. Smith, and R. E. Jewell, 2019: Using near-ground storm relative helicity in supercell tornado forecasting. *Wea. Forecasting*, **34**, 1417–1435, https://doi.org/10.1175/WAF-D-19-0115.1.

Davis, J. M., and M. D. Parker, 2014: Radar climatology of tornadic and nontornadic vortices in high-shear, low-cape environments in the mid-Atlantic and southeastern United States. *Wea. Forecasting*, **29**, 828–853, https://doi.org/10.1175/WAF-D-13-00127.1.

Demortier, A., D. Bozkurt, and M. Jacques-Coper, 2021: Identifying key driving mechanisms of heat waves in central Chile. *Climate Dyn.*, **57**, 2415–2432, https://doi.org/10.1007/s00382-021-05810-z.

dos Santos, L. O., E. L. Nascimento, and J. T. Allen, 2023: Discriminant analysis for severe storm environments in south-central Brazil. *Mon. Wea. Rev.*, **151**, 2659–2681, https://doi.org/10.1175/MWR-D-22-0347.1.

Durkee, J. D., and T. L. Mote, 2010: A climatology of warm-season mesoscale convective complexes in subtropical South America. *Int. J. Climatol.*, **30**, 418–431, https://doi.org/10.1002/joc.1893.

Ellis, K. N., D. Burow, K. N. Gassert, L. R. Mason, and M. S. Porter, 2020: Forecaster perceptions and climatological analysis of the influence of convective mode on tornado climatology and warning success. *Ann. Assoc. Amer. Geogr.*, **110**, 1075–1094, https://doi.org/10.1080/24694452.2019.1670042.

Falvey, M., and R. D. Garreaud, 2009: Regional cooling in a warming world: Recent temperature trends in the Southeast Pacific and along the west coast of subtropical South America (1979–2006). *J. Geophys. Res.*, **114**, D04102, https://doi.org/10.1029/2008JD010519.

Gensini, V. A., and H. E. Brooks, 2018: Spatial trends in United States tornado frequency. *npj Climate Atmos. Sci.*, **1**, 38, https://doi.org/10.1038/s41612-018-0048-2.

——, and L. Bravo de Guenni, 2019: Environmental covariate representation of seasonal U.S. tornado frequency. *J. Appl. Meteor. Climatol.*, **58**, 1353–1367, https://doi.org/10.1175/JAMC-D-18-0305.1.

——, C. Converse, W. S. Ashley, and M. Taszarek, 2021: Machine learning classification of significant tornadoes and hail in the United States using ERA5 proximity soundings. *Wea. Forecasting*, **36**, 2143–2160, https://doi.org/10.1175/WAF-D-21-0056.1.

González-Reyes, Á., M. Jacques-Coper, C. Bravo, M. Rojas, and R. Garreaud, 2023: Evolution of heatwaves in Chile since 1980. *Wea. Climate Extremes*, **41**, 100588, https://doi.org/10.1016/j.wace.2023.100588.

Grams, J. S., R. L. Thompson, D. V. Snively, J. A. Prentice, G. M. Hodges, and L. J. Reames, 2012: A climatology and comparison of parameters for significant tornado events in the United States. *Wea. Forecasting*, **27**, 106–123, https://doi.org/10.1175/WAF-D-11-00008.1.

Hanstrum, B. N., G. A. Mills, A. Watson, J. P. Monteverdi, and C. A. Doswell III, 2002: The cool-season tornadoes of California and southern Australia. *Wea. Forecasting*, **17**, 705–722, https://doi.org/10.1175/1520-0434(2002)017<0705:TCSTOC>2.0.CO;2.

Hare, S. R., and N. J. Mantua, 2000: Empirical evidence for North Pacific regime shifts in 1977 and 1989. *Prog. Oceanogr.*, **47**, 103–145, https://doi.org/10.1016/S0079-6611(00)00033-1.

Hersbach, H., and Coauthors, 2020: The ERA5 global reanalysis. *Quart. J. Roy. Meteor. Soc.*, **146**, 1999–2049, https://doi.org/10.1002/qj.3803.

Istrate, V., D. Podiuc, D. A. Sîrbu, E. Popescu, E. Sîrbu, and D. D. Popescu, 2023: Characteristics of convective parameters derived from rawinsonde and ERA5 data associated with hailstorms in northeastern Romania. *Meteorology*, **2**, 387–402, https://doi.org/10.3390/meteorology2030023.

Jacques-Coper, M., and R. D. Garreaud, 2015: Characterization of the 1970s climate shift in South America. *Int. J. Climatol.*, **35**, 2164–2179, https://doi.org/10.1002/joc.4120.

Kumjian, M. R., and Coauthors, 2020: Gargantuan hail in Argentina. *Bull. Amer. Meteor. Soc.*, **101**, E1241–E1258, https://doi.org/10.1175/BAMS-D-19-0012.1.

Lagos-Zúñiga, M., P. A. Mendoza, D. Campos, and R. Rondanelli, 2024: Trends in seasonal precipitation extremes and associated temperatures along continental Chile. *Climate Dyn.*, **62**, 4205–4222, https://doi.org/10.1007/s00382-024-07127-z.

Lopes, M. M., and E. L. Nascimento, 2024: Atmospheric environments associated with tornadoes in southern Brazil and neighboring areas as compared to other modes of convective hazards. *Climate Dyn.*, **62**, 3641–3667, https://doi.org/10.1007/s00382-023-07089-8.

Marín, J. C., B. S. Barrett, and D. Pozo, 2021: The tornadoes of 30–31 May 2019 in south-central Chile: Sensitivity to topography and SST. *Atmos. Res.*, **249**, 105301, https://doi.org/10.1016/j.atmosres.2020.105301.

Matsudo, C. M., and P. V. Salio, 2011: Severe weather reports and proximity to deep convection over northern Argentina. *Atmos. Res.*, **100**, 523–537, https://doi.org/10.1016/j.atmosres.2010.11.004.

Meehl, G. A., A. Hu, and B. D. Santer, 2009: The mid-1970s climate shift in the Pacific and the relative roles of forced versus inherent decadal variability. *J. Climate*, **22**, 780–792, https://doi.org/10.1175/2008JCLI2552.1.

Monteverdi, J. P., and J. Quadros, 1994: Convective and rotational parameters associated with three tornado episodes in northern and central California. *Wea. Forecasting*, **9**, 285–300, https://doi.org/10.1175/1520-0434(1994)009<0285:CARPAW>2.0.CO;2.

Moraes, F. D., F. E. Aquino, T. L. Mote, J. D. Durkee, and K. S. Mattingly, 2020: Atmospheric characteristics favorable for the development of mesoscale convective complexes in southern Brazil. *Climate Res.*, **80**, 43–58, https://doi.org/10.3354/cr01595.

Mulder, K. J., and D. M. Schultz, 2015: Climatology, storm morphologies, and environments of tornadoes in the British Isles: 1980–2012. *Mon. Wea. Rev.*, **143**, 2224–2240, https://doi.org/10.1175/MWR-D-14-00299.1.

Muñoz, R. C., C. D. Whiteman, R. D. Garreaud, J. A. Rutllant, and J. Hidalgo, 2022: Using commercial aircraft meteorological data to assess the heat budget of the convective boundary layer over the Santiago valley in central Chile. *Bound.-Layer Meteor.*, **183**, 295–319, https://doi.org/10.1007/s10546-021-00685-3.

Newman, M., and Coauthors, 2016: The Pacific decadal oscillation, revisited. *J. Climate*, **29**, 4399–4427, https://doi.org/10.1175/JCLI-D-15-0508.1.

Nunes, L. H., L. D. Bona, and D. H. Candido, 2011: Tornado and waterspout climatology in Brazil. *Sixth European Conf. on Severe Storms (ECSS 2011)*, Palma de Mallorca, Spain, 209, https://www.essl.org/ECSS/2011/programme/posters/209.pdf.

Piersante, J. O., K. L. Rasmussen, R. S. Schumacher, A. K. Rowe, and L. A. McMurdie, 2021: A synoptic evolution comparison of the smallest and largest MCSs in subtropical south America between spring and summer. *Mon. Wea. Rev.*, **149**, 1943–1966, https://doi.org/10.1175/MWR-D-20-0208.1.

Pilguj, N., M. Taszarek, J. T. Allen, and K. A. Hoogewind, 2022: Are trends in convective parameters over the United States and Europe consistent between reanalyses and observations? *J. Climate*, **35**, 3605–3626, https://doi.org/10.1175/JCLI-D-21-0135.1.

Pilorz, W., I. Laskowski, A. Surowiecki, M. Taszarek, and E. Lupikasza, 2024: Comparing ERA5 convective environments associated with hailstorms in Poland between 1948–1955 and 2015–2022. *Atmos. Res.*, **301**, 107286, https://doi.org/10.1016/j.atmosres.2024.107286.

Pozo, D., J. C. Marín, and F. Gutiérrez, 2023: Cloud properties of cold fronts affecting central Chile: Low and high freezing level storms. *Earth Space Sci.*, **10**, e2022EA002591, https://doi.org/10.1029/2022EA002591.

Quintana, J., and P. Aceituno, 2012: Changes in the rainfall regime along the extratropical west coast of South America (Chile): 30-43°S. *Atmósfera*, **25**, 1–22.

Rasmussen, K. L., M. D. Zuluaga, and R. A. Houze Jr., 2014: Severe convection and lightning in subtropical South America. *Geophys. Res. Lett.*, **41**, 7359–7366, https://doi.org/10.1002/2014GL061767.

Rodríguez, O., and J. Bech, 2021: Tornadic environments in the Iberian Peninsula and the Balearic Islands based on ERA5 reanalysis. *Int. J. Climatol.*, **41**, E1959–E1979, https://doi.org/10.1002/joc.6825.

Romatschke, U., and R. A. Houze Jr., 2010: Extreme summer convection in South America. *J. Climate*, **23**, 3761–3791, https://doi.org/10.1175/2010JCLI3465.1.

Romps, D. M., 2021: Accurate expressions for the dewpoint and frost point derived from the Rankine–Kirchhoff approximations. *J. Atmos. Sci.*, **78**, 2113–2116, https://doi.org/10.1175/JAS-D-20-0301.1.

Schauwecker, S., G. Palma, S. MacDonell, Á. Ayala, and M. Viale, 2022: The snowline and 0°C isotherm altitudes during precipitation events in the dry subtropical Chilean Andes as seen by citizen science, surface stations, and ERA5 reanalysis data. *Front. Earth Sci.*, **10**, 875795, https://doi.org/10.3389/feart.2022.875795.

Schumacher, R. S., and Coauthors, 2021: Convective-storm environments in subtropical South America from high-frequency soundings during RELAMPAGO-CACTI. *Mon. Wea. Rev.*, **149**, 1439–1458, https://doi.org/10.1175/MWR-D-20-0293.1.

Schwarzkopf, M. L. A., 1988: Climatology of the effects of severe convection over Argentina. Ph.D. dissertation, Universidad de Buenos Aires, 160 pp, https://bibliotecadigital.exactas.uba.ar/download/tesis/tesis_n2211_AltingerdeSchwarzkopf.pdf.

Sherburn, K. D., and M. D. Parker, 2014: Climatology and ingredients of significant severe convection in high-shear, low-cape environments. *Wea. Forecasting*, **29**, 854–877, https://doi.org/10.1175/WAF-D-13-00041.1.

——, ——, J. R. King, and G. M. Lackmann, 2016: Composite environments of severe and nonsevere high-shear, low-CAPE convective events. *Wea. Forecasting*, **31**, 1899–1927, https://doi.org/10.1175/WAF-D-16-0086.1.

Shikhov, A. N., A. V. Chernokulsky, A. A. Sprygin, and Y. I. Yarinich, 2022: Estimation of convective atmospheric instability during squalls, tornadoes, and large hail events from satellite observations and ERA5 reanalysis data. *Atmos. Oceanic Opt.*, **35**, 793–801, https://doi.org/10.1134/S1024856022060227.

Silva Dias, M. A. F., 2011: An increase in the number of tornado reports in Brazil. *Wea. Climate Soc.*, **3**, 209–217, https://doi.org/10.1175/2011WCAS1095.1.

Taszarek, M., J. T. Allen, M. Marchio, and H. E. Brooks, 2021a: Global climatology and trends in convective environments

from ERA5 and rawinsonde data. *npj Climate Atmos. Sci.*, **4**, 35, https://doi.org/10.1038/s41612-021-00190-x.

——, N. Pilguj, J. T. Allen, V. Gensini, H. E. Brooks, and P. Szuster, 2021b: Comparison of convective parameters derived from ERA5 and MERRA-2 with rawinsonde data over Europe and north America. *J. Climate*, **34**, 3211–3237, https://doi.org/10.1175/JCLI-D-20-0484.1.

Thompson, R. L., R. Edwards, J. A. Hart, K. L. Elmore, and P. Markowski, 2003: Close proximity soundings within supercell environments obtained from the rapid update cycle. *Wea. Forecasting*, **18**, 1243–1261, https://doi.org/10.1175/1520-0434(2003)018<1243:CPSWSE>2.0.CO;2.

——, ——, C. M. Mead, and S. P. Center, 2004: An update to the supercell composite and significant tornado parameters. Preprints, *22nd Conf. on Severe Local Storms*, Hyannis, MA, Amer. Meteor. Soc., P8.1, https://ams.confex.com/ams/pdfpapers/82100.pdf.

——, B. T. Smith, J. S. Grams, A. R. Dean, and C. Broyles, 2012: Convective modes for significant severe thunderstorms in the contiguous United States. Part II: Supercell and QLCS tornado environments. *Wea. Forecasting*, **27**, 1136–1154, https://doi.org/10.1175/WAF-D-11-00116.1.

Tippett, M. K., J. T. Allen, V. A. Gensini, and H. E. Brooks, 2015: Climate and hazardous convective weather. *Curr. Climate Change Rep.*, **1**, 60–73, https://doi.org/10.1007/s40641-015-0006-6.

Veloso-Aguila, D., K. L. Rasmussen, and E. D. Maloney, 2024: Tornadoes in southeast South America: Mesoscale to planetary-scale environments. *Mon. Wea. Rev.*, **152**, 295–318, https://doi.org/10.1175/MWR-D-22-0248.1.

Vicencio, J., and Coauthors, 2020: The Chilean tornado outbreak of May 2019: Synoptic, mesoscale, and historical contexts. *Bull. Amer. Meteor. Soc.*, **102**, E611–E634, https://doi.org/10.1175/BAMS-D-19-0218.1.

Wade, A. R., and M. D. Parker, 2021: Dynamics of simulated high-shear, low-CAPE supercells. *J. Atmos. Sci.*, **78**, 1389–1410, https://doi.org/10.1175/JAS-D-20-0117.1.

Wikipedia, 2019: Anexo: Tornados en Chile. Accessed 20 January 2024, https://es.wikipedia.org/wiki/Anexo:Tornados_en_Chile.